Wireless Holographic Image Communications Relying on Unequal Error Protected Bitplanes

Yongkai Huo[12], Péter Tamás Kovács[3], Thomas J. Naughton[4] and Lajos Hanzo[2], *Fellow, IEEE*
[1]College of Computer Science&Software Engineering, Shenzhen University, China.
[2]School of ECS, University of Southampton, UK.
[3]Holografika Kft, Budapest Hungary.
[4]Department of Computer Science, National University of Ireland, Maynooth, County Kildare, Ireland.
Email: ykhuo[1]@szu.edu.cn, {yh3g09[2], lh[2]}@ecs.soton.ac.uk, p.kovacs[3]@holografika.com, tomn[4]@cs.nuim.ie.com

***Abstract*—Holography is considered to be one of the most promising techniques of goggle-free visualization of the near-future. We consider wireless transmission of digital holograms, which are partitioned into multiple bitplanes that are then independently encoded by a forward error correction (FEC) code for transmission over wireless channels. The coding rates of these bitplanes will be optimized at the transmitter for the sake of achieving an improved holographic peak signal-to-noise ratio (PSNR) at the receiver. Our simulation results show that up to 2.6 dB of E_b/N_0 or 12.5 dB of PSNR improvements may be achieved, when employing a recursive systematic convolutional (RSC) code.**

I. Introduction

Holography has been widely researched since its invention by Gabor [1]. We commence by introducing the holography concept, followed by the current state-of-the-art in its compression and transmission. We continue by outlining the motivation and focus of our paper and present its structure.

A. Holography

Holography [1] constitutes a sophisticated technique of recording and reconstructing both the amplitude and phase of an optical wavefront relying on the interference and diffraction imposed by an object on visible light. Holography[1] [1], including optical holography, computer generated holography (CGH) and digital holography (DH) are being actively researched at the time of writing [2]–[6]. In [4], CGHs were generated using a small number of multiview images captured by appropriately arranged cameras. An efficient generation of the CGH was proposed in [6]. The European Real 3D research project [2], [7] aimed for capturing both 3D and 4D real-world objects as well as for the processing and display of digital holography.

1) Optical Holography: Optical holography allows the holographic images to be recorded and reconstructed using a white-light illumination source [8] or a illuminating laser [9]. According to the reconstruction method, holograms may be classified as reflection [8] and transmission holograms [9]. In this treatise, we focus on the transmission holograms, which may be recorded and reconstructed as in Fig. 2. *Optical holography entails the family of techniques that record a hologram using traditional acetate-based film and then reconstructs the image optically using an illumination light.*

2) Computer Generated Holography: CGH was firstly proposed by Brown and Lohmann in 1966 [10], [11], which allows us to generate holograms with the aid of sophisticated mathematical manipulations of an object that does not physically exist but can be described in mathematical terms. *Hence, CGH refers to the family of techniques that generate a hologram from virtual objects using mathematical manipulations and then reconstruct the image optically using classic laser illumination methods* [9].

3) Digital Holography: Goodman and Lawrence [12] proposed the principle of digital holography [13], which yields images reconstructed with the aid of computations from a digitized Fourier hologram, that was electronically detected by a vidicon camera [12] from an optically recorded hologram. Based on this principle, the fundamental theory of digital holography was conceived by Yaroslavskii and Merzlyakov in 1980 [14]. *In a nutshell, digital holography (DH) refers to the class of techniques that record a hologram digitally and reconstruct the image using numerical manipulations.*

B. Compression and Transmission

Holography has been widely researched for diverse applications [15], [16], such as deformation analysis [17], communications [18] and microscopy [13] etc. Since digital holograms, including the CGH and DH holograms, are stored in digital form, suitable compression and transmission techniques have to be investigated for the sake of reducing the storage required in a hard-drive for example, or the transmission bandwidth and the transmission power required for distributing the holograms [19].

A number of compression techniques were discussed in [20], [21], including classic lossless compression, quantization, Fourier-domain processing, wavelet analysis etc. The lossy compression of phase-shift based digital holograms was investigated in [22], where both the real and imaginary streams were quantized, followed by a bit-packing operation. The wavelet-like basis functions, namely the so-called Fresnelets were investigated in [23], [24]. Wavelet analysis was employed in [25] for the compression of complex-valued digital

The financial support of the European Research Council's (ERC) Advanced Fellow Grant Beam-me-up is gratefully acknowledged. No funding from EPSRC was received.

This paper was accepted for publication in the IEEE Transactions on Vehicular Technology on the 6th of January 2017.

[1]The word 'holography' originated from the Greek words 'holos' meaning whole or entire and 'graphein' meaning to write.

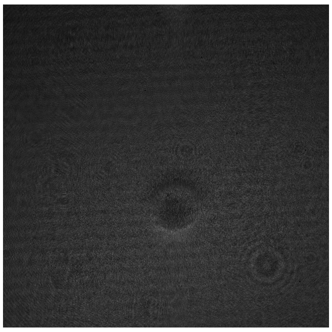

(a) Hologram of a Coil

(b) Jockey Image

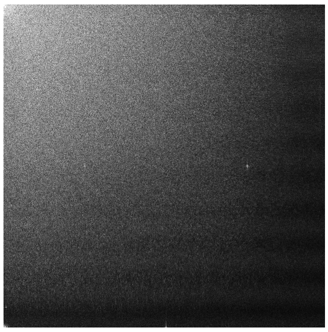

(c) DCT domain, Coil hologram

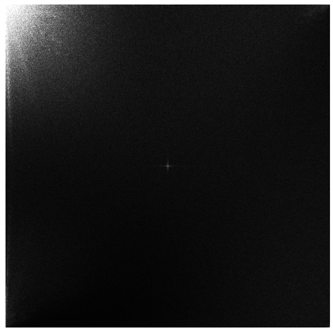

(d) DCT domain, Jockey Image

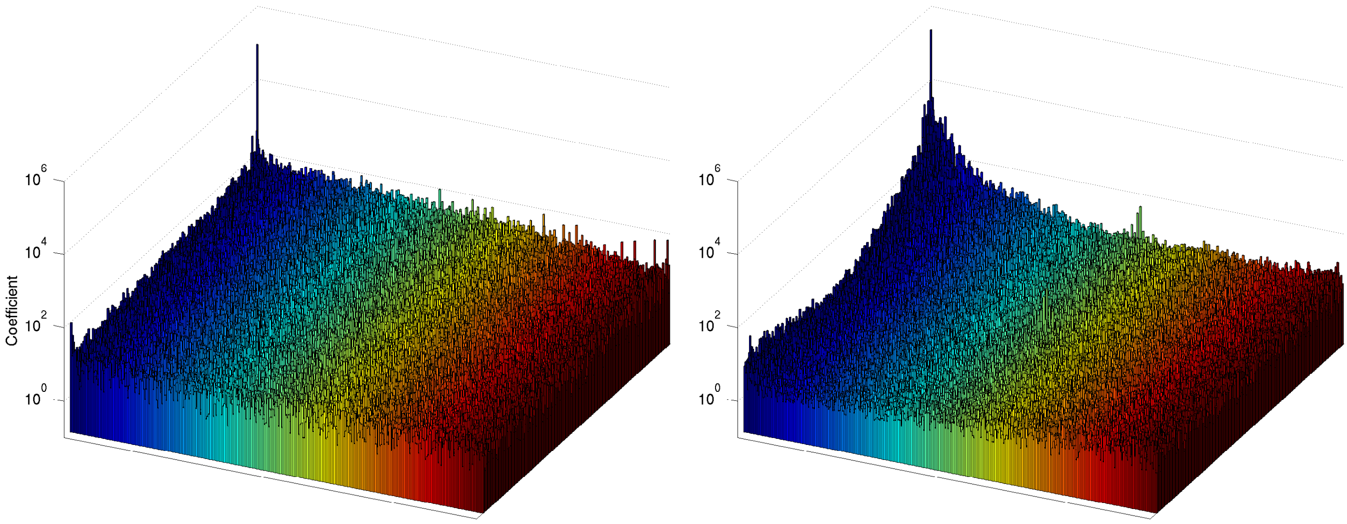

(e) DCT Coefficients, Coil hologram vs Jockey Image

Figure 1: Comparison of the hologram of a Coil to a Jockey image.

holograms of three-dimensional real-world objects, where the thresholding and quantization of the wavelet coefficients was invoked, followed by the lossless encoding of the quantized data. In [26], the Wavelet-Bandelets transform was employed for hologram compression. The widely known scalable video coding method of [27] was employed in [28] for compressing holographic video.

However, there is a paucity of literature on the transmission of digital holograms. A wireless holographic video transmission system was proposed in [29], where the holograms were transformed into a bitstream, and then transmitted over both wireless LAN and Bluetooth. In [30], the authors investigated the transmission of holograms through a multi-mode optical fiber by shaping the wavefront of the input beam with the aid of a spatial light modulator. Transmission of holograms and 3D image reconstruction using white LED light was investigated in [31]. The authors of [32] proposed a method to transmit CGH using an infrared-rays, where the hologram was compressed before transmission.

C. *Our Motivation*

The distribution of digital hologram pixels is rather different from that of traditional photographic image pixels [24], [33], [34], as exemplified in Fig. 1 portraying the hologram of a simple Coil and a Jockey image. The visual comparison of a hologram and of a traditional image is shown by Fig. 1a and Fig. 1b, while corresponding discrete cosine transform (DCT) coefficients are compared in Figs. 1c, 1d and 1e. As displayed in Fig. 1e, high valued DCT coefficients of the correlated Jockey image tend to be in the top left corner associated with the low-frequency components, which indicates that a compressed version of the Jockey image may be represented by a small faction of the coefficients, thereby achieving high compression. In contrast to the Jockey image, the DCT coefficients of the Coil hologram tend to be more uniformly scattered over the whole DCT coefficient plane. Hence the traditional image compression techniques, such as the Joint Photographic Experts Group's (JPEG) schemes [35] and the intra-frame compression mode of H.264/AVC [36] are inefficient for digital uncorrelated holograms.

D. Our Focus

As discussed above, digital holograms may be widely utilized in future applications. However, apart from [30], the transmission of digital holograms has rarely been researched. Hence we embark on tackling this open problem by investigating the transmission of digital holograms through wireless channels. Furthermore, since no widely acclaimed compression algorithms have been developed in the open literature, we directly transmit uncompressed holograms with the objective of reconstructing the original high quality decoded digital holograms at the receiver. Explicitly, we propose an optimized unequal error protection based forward error correction (Opt-UEP-FEC) coded system, where the holograms will be transmitted bitplane by bitplane after forward error correction (FEC). We will optimize unequal error protection (UEP) [37] rates of the bitplanes for the sake of maximizing the quality of the received digital holograms. Note that our previous work [37]–[39] optimized the coding rates of the different layers in scalable video, where the less important layers rely on the more important layers for their decoding. By contrast, in this contribution, we optimize the coding rates of different bitplanes, which are independent of each other for decoding.

Hence the novelty of this paper is listed as follows:

- We study the transmission of uncompressed holograms based on unequal error protected bitplanes.
- We optimize the coding rates of unequal FEC protection. Our solution may be applied to arbitrary channels, modulation arrangements and to non-iterative FEC schemes.
- Substantial system performance improvements have been achieved compared to conventional equal error protection (EEP) schemes.

The rest of the paper is organized as follows. Section II will briefly introduce the basic principles of both optical holography, as well as of CGH, and DH. Then the architecture of the proposed system will be presented in Section III, followed by the proposed coding rate optimization in Section IV. Then the system's performance will be characterized in Section V. Finally, Section VI concludes the paper.

II. Basics of Holography

A. Recording

The optical set-up of hologram recording is illustrated in Fig. 2a, where an object, a coherent light source - such as a laser, as well as mirrors, lenses and a recording medium are employed. The laser is split into a pair of partial waves by the beam splitter (BS), namely the waves E_I and E_R of Fig. 2a. The wave E_I of Fig. 2a, which is referred to as the illumination wave, illuminates the object and it is scattered by the object's surface. The scattered wave, which is also referred

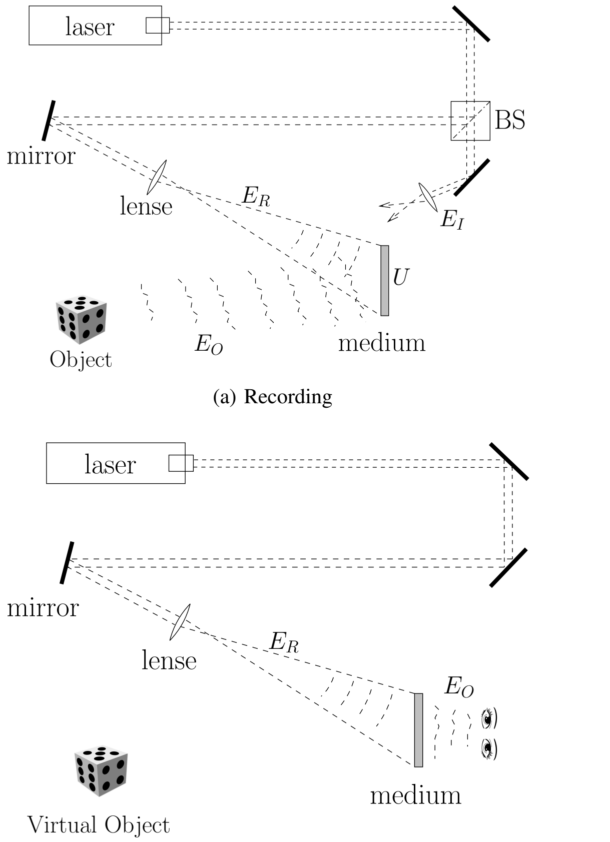

(a) Recording

(b) Optical Reconstruction

Figure 2: Optical set-up of holography

to as the object wave, E_O is then reflected onto the recording medium U of Fig. 2a. The wave E_R, which is also referred to as the reference wave, illuminates the recording medium directly. Finally, the interference pattern created by this pair of waves will be recorded by the medium U, which is the resultant hologram. A conventional photographic plate may be employed as the recording medium of Fig. 2a for optical hologram recording. By contrast, a CCD may be invoked for digital hologram recording.

We assume that the complex-valued amplitude of the object wave E_O of Fig. 2a is described by

$$E_O\left(w,h\right) = a_O\left(w,h\right) \cdot \exp\left[i\varphi_O\left(w,h\right)\right] \tag{1}$$

where the real-valued amplitude is a_o and the phase is denoted by φ_o. The complex-valued amplitude of the reference wave E_R of Fig. 2a is described by

$$E_R\left(w,h\right) = a_R\left(w,h\right) \cdot \exp\left[i\varphi_R\left(w,h\right)\right] \tag{2}$$

where the real-valued amplitude is denoted by a_R and the phase by φ_R. Then the intensity of the interference pattern of the two waves at the surface of the recording medium U of Fig. 2a can be expressed as

$$U\left(w,h\right) = \left|E_O\left(w,h\right) + E_R\left(w,h\right)\right|^2 \tag{3}$$

For CGH, the hologram is created by calculating Eqs. (1) to (3), where the mathematical model of the object is known.

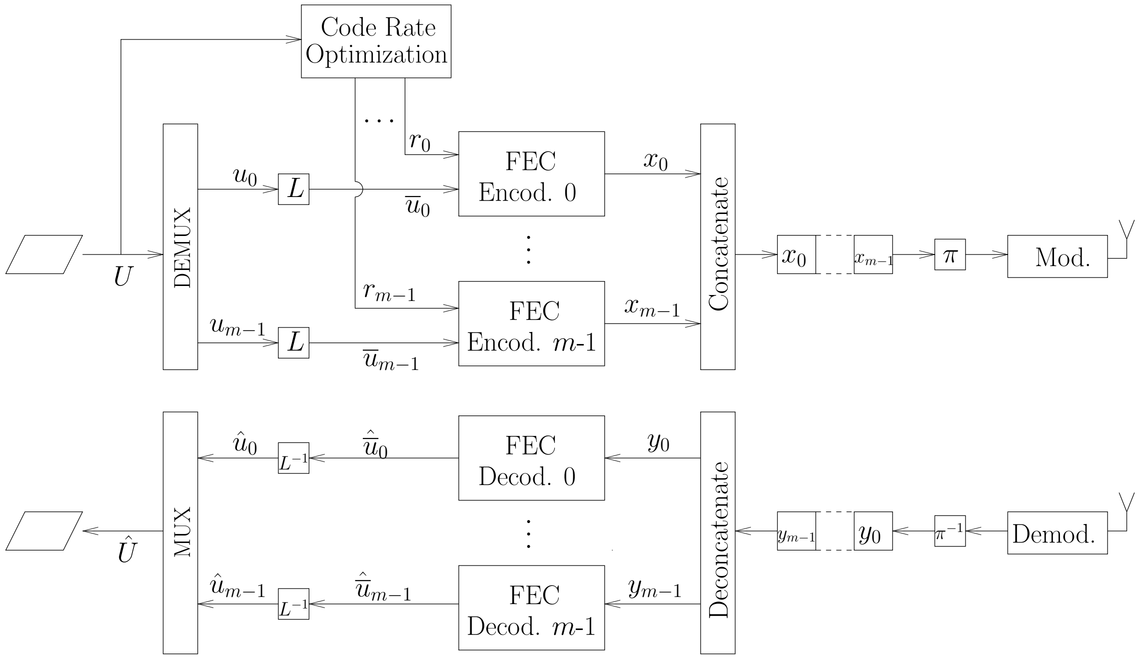

Figure 3: Block diagram of the proposed Opt-UEP-FEC system, where m is the bit-depth of the hologram, while $r_0, \cdots, r_{m-1}$ represent the code rates of the FEC encoders $0, \cdots, m-1$, respectively. The "Code Rate Optimization" block will be detailed in Section IV.

More details about the CGH may be found in [40], [41].

B. Reconstruction

The optical reconstruction set-up is illustrated in Fig. 2b, where a coherent laser light source, mirrors, lenses and a hologram are employed. The reference wave E_R illuminates the hologram U, which results in a virtual image, that may be viewed by the observer.

The amplitude transmittance $H(w,h)$ of the recording medium is proportional to the intensity $U(x,y)$ of the hologram, which may be expressed as

$$H(w,h) = H_0 + \beta\tau \cdot U(w,h) \tag{4}$$

where β represents the slope of the amplitude transmittance versus the exposure characteristic of the light sensitive material, while τ is the exposure time and H_0 is the amplitude representing the unexposed plate [15]. The associated hologram reconstruction can be described mathematically as the product of the amplitude transmittance $H(w,h)$ and the reference wave E_R of Fig. 2b, namely $E_R(w,h)\,H(w,h)$.

For CGH, the digital hologram is firstly printed on film, which will then be optically reconstructed. For DH, the hologram will be numerically reconstructed by simulating the optical reconstruction process [15], [40], [41].

III. System Architecture

In this section, we introduce the proposed unequal error protection (UEP) based FEC coded (Opt-UEP-FEC) system conceived for holographic communications, whose system model is detailed in Fig. 3. We focus on the general architecture of the transmitter and receiver, while the "Code Rate Optimization" block will be detailed in Section IV. Let us commence by defining the notations as in Table I.

Symbol	Definition
U	the original hologram, as displayed in Fig. 3
m	number of bits/pixel for the hologram U
u_i	the i^{th} bitplane of the hologram U
$\overline{u}_i$	the bit sequence linearly indexed[2] from the bitplane u_i
r_i	FEC coding rate of the bitplane u_i
x_i	the FEC encoded sequence of the bitplane u_i
y_i	the received version of sequence x_i
$\hat{\overline{u}}_i$	the decoded version of bit sequence $\overline{u}_i$
$\hat{u}_i$	the decoded version of bit sequence u_i
$\hat{U}$	the reconstructed hologram at the receiver

Table I: Symbol definition, where $0 \leq i < m$ indicates the bitplane index.

A. Transmitter Model

At the transmitter of Fig. 3, the original hologram U is de-multiplexed into the classic bitplanes $u_0, \cdots, u_{m-1}$ by the *DEMUX* block, where u_0/u_{m-1} represents the most/least significant bitplane[3]. Meanwhile, the original hologram U is

[3] Assume a 2D image has m-bits/pixel, where each pixel may be split into m bits. All the bits having the same significance are collected in a bitplane.

input to the "Code Rate Optimization" block, which will generate the optimized coding rates $r_0, \cdots, r_{m-1}$ for the bitplanes $u_0, \cdots, u_{m-1}$, respectively. Afterwards, each bitplane u_i $(0 \le i < m)$ is encoded as follows:

1) The bitplane u_i will be linearly indexed to generate the sequence $\overline{u}_i$ by the block L.
2) The resultant sequence $\overline{u}_i$ is then encoded by the FEC encoder i, which generates the encoded bit sequence x_i.

Finally, the bit sequences $x_0, \cdots, x_{m-1}$ are concatenated into a joint bitstream for transmission. The interleaver π of Fig. 3 is employed for interleaving the joint bitstream before the modulation and transmission over *non-dispersive uncorrelated Rayleigh fading wireless channels*. Although we will employ a simple binary phase-shift keying (BPSK) modulator in the "Mod." block, arbitrary transceivers may be applied in our proposed system.

B. Receiver Model

At the receiver, BPSK demodulation, deinterleaving and deconcatenation are performed, as seen in Fig. 3, which generate the soft information $y_0, \cdots, y_{m-1}$ for the bitplanes $u_0, \cdots, u_{m-1}$, respectively. Then each bitplane u_i $(0 \le i < m)$ is estimated as follows:

1) The soft information y_i is decoded by the FEC decoder i generating the bit sequence $\hat{\overline{u}}_i$, which is the estimated version of bit sequence $\overline{u}_i$.
2) The sequence $\hat{\overline{u}}_i$ will then be reformatted to the bitplane $\hat{u}_i$ by the the block L^{-1}, where $\hat{u}_i$ is the estimated version of the bitplane u_i.

Finally, the estimated bitplanes $\hat{u}_0, \cdots, \hat{u}_{m-1}$ are reconstructed into the final estimated hologram $\hat{U}$ by the "MUX" block.

IV. Coding Rate Optimization

In this section, we detail the "Code Rate Optimization" block of Fig. 3. This "Code Rate Optimization" block has the task of finding the specific FEC coding rates $r_0, \cdots, r_{m-1}$ required for encoding the different-significance bitplanes $u_0, \cdots, u_{m-1}$. We denote the position of a specific pixel by $\rho = (w, h)$ in the intensity hologram frame for notational simplicity. Note that real valued numbers are utilized for representing a pixel in an intensity hologram, while complex numbers may be utilized in amplitude holograms and phase holograms. For the sake of simplicity, the intensity hologram is utilized here, but our algorithm may be readily employed also for complex-valued holograms. Let us commence by defining the notations in Table II based on Section III.

The coding rates $r_0, \cdots, r_{m-1}$ of Fig. 3 aim for maximizing the quality of the image reconstructed from the estimated hologram $\hat{U}$ at the receiver. However, as discussed in Section II, the reconstruction process involves multiple parameters, such as the wavelength of the laser, which makes the optimization of the reconstructed image at the transmitter a challenging task. In this paper, our objective is to maximize the peak signal-to-noise ratio (PSNR) of the estimated hologram $\hat{U}$, which represents the most popular objective video quality metric of the reconstructed image [42]. Defining the PSNR of the estimated hologram $\hat{U}$ as $PSNR_U$, our objective function (OF) invoked for maximizing the quality of this hologram may be formulated as

Symbol	Definition
W	the width of the hologram
H	the height of the hologram
R	overall coding rate of the system
$U(\rho)$	the pixel at position $\rho = (w, h)$ of the hologram U, namely $U(w, h)$
$\hat{U}(\rho)$	the pixel at position (w, h) of the received and reconstructed hologram
$u_i(\rho)$	the i^{th} bit of the pixel $U(\rho)$, namely the bit at position (w, h) of the bitplane u_i
$\hat{u}_j(\rho)$	the j^{th} bit of the pixel $\hat{U}(\rho)$
$p[u_i(\rho) = 1]$	indicates the probability that the bit $u_i(\rho)$ is 1
$p[\hat{u}_j(\rho) = 1]$	indicates the probability that the bit $\hat{u}_j(\rho)$ is 1

Table II: Symbol definition, where $0 \le i < m$, $0 \le j < m$ indicate the bitplane index.

$$\underset{r_0, \cdots, r_{m-1}}{\arg} \max \left\{ E\left(PSNR_U\right) \right\} \tag{5}$$

where the $PSNR_U$ of the reconstructed hologram $\hat{U}$ may be calculated as

$$\begin{aligned} PSNR_U &= 10 \cdot \log_{10} \left\{ \frac{\left(2^m - 1\right)^2}{MSE} \right\} dB \\ MSE &= \frac{1}{W \cdot H} \sum_{w=0}^{H-1} \sum_{h=0}^{W-1} \left[U(\rho) - \hat{U}(\rho) \right]^2 \end{aligned} \tag{6}$$

where the MSE is calculated based on the original hologram U and the reconstructed hologram $\hat{U}$.

We note that MSE is inversely proportional to $PSNR_U$. By assuming that all pixels of U obey an identical distribution, our objective function of Eq. (5) may be expressed as

$$\underset{r_0, \cdots, r_{m-1}}{\arg} \min \left\{ \sum_{w=0}^{H-1} \sum_{h=0}^{W-1} E \left[U(\rho) - \hat{U}(\rho) \right]^2 \right\} \tag{7}$$

subject to the overall coding rate constraint of

$$\sum_{i=0}^{m-1} \frac{1}{r_i} = \frac{m}{R} \tag{8}$$

The hologram $\hat{U}$ of Eq. (7) is reconstructed from the FEC-decoded bitplanes $\hat{U}_0, \cdots, \hat{U}_{m-1}$. Hence the estimated hologram $\hat{U}$ is jointly determined by the transceivers and FEC codecs of Fig. 3, as well as by the related FEC coding rates $r_0, \cdots, r_{m-1}$. These components of Fig. 3 cannot be analytically characterized, especially when considering diverse transceivers and FEC codecs may be employed. In Section IV-A, we will firstly propose our solution for characterizing the "demodulation - FEC decoding" operations at the receiver of Fig. 3 with the assistance of a Lookup table (LUT). Then, in Sections IV-B and IV-C the OF of Eq. (7) will be cast in form of a multi-dimensional optimization problem, which will determine the optimal FEC coding rates $r_0, \cdots, r_{m-1}$ of Fig. 3. Finally, Section IV-D discusses the complexity issues imposed by the proposed techniques.

A. Lookup Table

Again, the "demodulation - FEC decoding" operations[4] of Fig. 3 cannot be analytically characterized for diverse system configurations, such as different transceivers, FEC generator polynomials, decoding metrics etc [37]. In our analysis, we consider the specific scenario that the m FEC codecs of Fig. 3 are identical for the sake of simplicity. We model the "demodulation - FEC decoding" operations as a function of both the channel SNR and the coding rate r, which generates a specific BER at its output. The following LUT is created correspondingly:

- $T\left(snr, r\right)$: The BER value of the decoded sequence after the "demodulation - FEC decoding" operations, where r represents the coding rate of the FEC codec. For example, $T\left(snr, r_i\right)$ returns the BER of the sequence $\hat{\bar{u}}_i$, namely that of the bitplane $\hat{u}_i$, when the FEC codec i has the coding rate r_i. Since this LUT relies both on the snr and on r, it may be stored in a three-dimensional memory. The LUT's memory requirements will be detailed in Section IV-D.

B. Derivation of the Objective Function

Based on the discussions above, for the holographic pixel $\rho = (w, h)$, we have the following expressions

- The pixels $U(\rho)$ and $\hat{U}(\rho)$ may be readily formulated as

$$\begin{aligned} U(\rho) &= \sum_{i=0}^{m-1} 2^i u_i\left(\rho\right) \\ \hat{U}(\rho) &= \sum_{i=0}^{m-1} 2^i \hat{u}_i\left(\rho\right) \end{aligned} \tag{9}$$

- The probability that the reconstructed bit $\hat{u}_j\left(\rho\right)$ is 1 may be expressed as $p\left[\hat{u}_j\left(\rho\right) = 1\right]$. According to the definition of the BER LUT $T\left(snr, r\right)$, the probability $p\left[\hat{u}_j\left(\rho\right) = 1\right]$ consists of the probability $p\left[u_j\left(\rho\right) = 1\right] \cdot \left[1 - T\left(snr, r_j\right)\right]$ indicating that the correctly decoded bit $\hat{u}_j\left(\rho\right)$ is 1 and the probability $\left[1 - p\left[u_j\left(\rho\right) = 1\right]\right] \cdot T\left(snr, r_j\right)$ indicating that the reconstructed bit $\hat{u}_j\left(\rho\right)$ is erroneous. Overall, the probability $p\left[\hat{u}_j\left(\rho\right) = 1\right]$ may be expressed as

$$\begin{aligned} p\left[\hat{u}_j\left(\rho\right) = 1\right] = &\left[1 - p\left[u_j\left(\rho\right) = 1\right]\right] \cdot T\left(snr, r_j\right) \\ &+ p\left[u_j\left(\rho\right) = 1\right] \cdot \left[1 - T\left(snr, r_j\right)\right] \end{aligned} \tag{10}$$

For the holographic pixel $\rho = (w, h)$, the expectation $E\left[U(\rho) - \hat{U}(\rho)\right]^2$ of Eq. (7) may be expressed as

$$\begin{aligned} &E\left[U(\rho) - \hat{U}(\rho)\right]^2 \\ &= E\left[U^2(\rho)\right] - 2E\left[U(\rho) \cdot \hat{U}(\rho)\right] + E\left[\hat{U}^2(\rho)\right] \end{aligned} \tag{11}$$

The component $E\left[U^2(\rho)\right]$ of Eq. (11) may be further formulated as

$$\begin{aligned} E\left[U^2(\rho)\right] &= E\left[\sum_{i=0}^{m-1} 2^i u_i\left(\rho\right)\right]^2 \\ &= \sum_{i=0}^{m-1}\sum_{j=0}^{m-1} 2^{i+j} \cdot E\left[u_i(\rho) \cdot u_j(\rho)\right] \end{aligned} \tag{12}$$

Similarly, for the components $E\left[\hat{U}^2(\rho)\right]$ and $E\left[U(\rho) \cdot \hat{U}(\rho)\right]$ of Eq. (11) we arrive at

$$\begin{aligned} E\left[\hat{U}^2(\rho)\right] &= E\left[\sum_{i=0}^{m-1} 2^i \hat{u}_i\left(\rho\right)\right]^2 \\ &= \sum_{i=0}^{m-1}\sum_{j=0}^{m-1} 2^{i+j} \cdot E\left[\hat{u}_i(\rho) \cdot \hat{u}_j(\rho)\right] \end{aligned} \tag{13}$$

$$\begin{aligned} E\left[U(\rho) \cdot \hat{U}(\rho)\right] &= E\left[\sum_{i=0}^{m-1} 2^i u_i\left(\rho\right) \cdot \sum_{j=0}^{m-1} 2^j \hat{u}_j\left(\rho\right)\right] \\ &= \sum_{i=0}^{m-1}\sum_{j=0}^{m-1} 2^{i+j} \cdot E\left[u_i(\rho) \cdot \hat{u}_j(\rho)\right] \end{aligned} \tag{14}$$

By substituting Eqs. (12), (13) and (14) into Eq. (11), the expectation $E\left[U(\rho) - \hat{U}(\rho)\right]^2$ of Eq. (7) may be reformulated as

$$\begin{aligned} E\left[U(\rho) - \hat{U}(\rho)\right]^2 = \sum_{i=0}^{m-1}\sum_{j=0}^{m-1} 2^{i+j} \cdot \\ \left\{E\left[u_i(\rho) \cdot u_j(\rho)\right] - 2E\left[u_i(\rho) \cdot \hat{u}_j(\rho)\right] + E\left[\hat{u}_i(\rho) \cdot \hat{u}_j(\rho)\right]\right\} \end{aligned} \tag{15}$$

Since we have $u_i(\rho) \in \{0, 1\}$ and $u_j(\rho) \in \{0, 1\}$, the expectation $E\left[u_i(\rho) \cdot u_j(\rho)\right]$ of Eq. (15) may be expressed as

$$E\left[u_i(\rho) \cdot \hat{u}_j(\rho)\right] = p\left[u_i\left(\rho\right) = 1\right] \cdot p\left[\hat{u}_j\left(\rho\right) = 1\right] \tag{16}$$

For $i = j$ and $u_i\left(\rho\right) = 1$, the probability $p\left[\hat{u}_j\left(\rho\right) = 1\right]$ of Eq. (16) represents the likelihood of the bit $u_i\left(\rho\right)$ being correctly decoded, which is given by[5] $\left[1 - T\left(snr, r_i\right)\right]$. Hence, we arrive at

$$\begin{aligned} &E\left[u_i(\rho) \cdot \hat{u}_j(\rho)\right] \\ &= \begin{cases} p\left[u_i\left(\rho\right) = 1\right] \cdot \left[1 - T\left(snr, r_i\right)\right], & i = j \\ p\left[u_i\left(\rho\right) = 1\right] \cdot p\left[\hat{u}_j\left(\rho\right) = 1\right], & i \neq j \end{cases} \end{aligned} \tag{17}$$

[4]Arbitrary modulation schemes and non-iterative FEC may be readily applied.

[5]Note that the bitplane u_i is encoded by the FEC encoder i of Fig. 3 using the coding rate r_i.

Similarly, for the expectations $E\left[u_i(\rho)\cdot u_j(\rho)\right]$ and $E\left[\hat{u}_i(\rho)\cdot \hat{u}_j(\rho)\right]$ of Eq. (15) we have

$$E\left[u_i(\rho)\cdot u_j(\rho)\right]=\begin{cases} p\left[u_i\left(\rho\right)=1\right], & i=j \\ p\left[u_i\left(\rho\right)=1\right]\cdot p\left[u_j\left(\rho\right)=1\right], & i\neq j \end{cases} \quad (18)$$

$$E\left[\hat{u}_i(\rho)\cdot \hat{u}_j(\rho)\right]=\begin{cases} p\left[\hat{u}_i\left(\rho\right)=1\right], & i=j \\ p\left[\hat{u}_i\left(\rho\right)=1\right]\cdot p\left[\hat{u}_i\left(\rho\right)=1\right], & i\neq j \end{cases} \quad (19)$$

By substituting Eqs. (10), (17), (18) and (19) into Eq. (15), the component $E\left[U(w,h)-\hat{U}(w,h)\right]^2$ in the OF of Eq. (7) may be expressed as in Eq. (20), where $p\left[\hat{u}_i\left(\rho\right)=1\right]$ is formulated by $p\left[u_j\left(\rho\right)=1\right]$ and $T\left(snr,r_j\right)$ is given in Eq. (10).

C. Optimal Rates

Three components are involved in the expression of $E\left[U(\rho)-\hat{U}(\rho)\right]^2$ in Eq. (20), namely the snr, the coding rates $r_0,\cdots,r_{m-1}$ and the source distribution probability $p\left[u_i\left(\rho\right)=1\right]$, where $p\left[u_i\left(\rho\right)=1\right]$ may be readily obtained by scanning the source hologram U. We strike a tradeoff between the performance attained and the complexity imposed by assuming that all bits of the bitplane u_i $(0\leq i<m)$ obey an identical distribution. Then Eq. (20) is equivalent to Eq. (21), where $\forall$ indicates an arbitrary pixel-position in the bitplane u_i and $p\left[\hat{u}_i\left(\forall\right)=1\right]$ is calculated as

$$\begin{aligned} p\left[\hat{u}_i\left(\forall\right)=1\right]&=\left[1-p\left[u_i\left(\forall\right)=1\right]\right]\cdot T\left(snr,r_i\right)\\ &\quad+p\left[u_i\left(\forall\right)=1\right]\cdot\left[1-T\left(snr,r_i\right)\right] \end{aligned} \quad (22)$$

Based on Eq. (21), the OF of Eq. (5) may be expressed as

$$\underset{r_0,\cdots,r_{m-1}}{\arg}\min\left\{E\left[U(\forall)-\hat{U}(\forall)\right]^2\right\} \quad (23)$$

subject to the overall coding rate constraint of

$$\sum_{i=0}^{m-1}\frac{1}{r_i}=\frac{m}{R} \quad (24)$$

Given a specific snr, the BER LUT $T\left(snr,r_i\right)$ can be readily found by fitting a mathematical function. Finally, we may obtain the optimized coding rates $r_0,\cdots,r_{m-1}$ by solving the multi-dimensional optimization problem formulated in Eq. (23) under the condition of Eq. (24) [6].

The distribution of $p\left[u_i\left(\forall\right)=1\right]$ $(0\leq i<m)$ is exemplified in Fig. 4. To elaborate a little further, we consider the example of Fig. 4a, where we have $p\left[u_i\left(\forall\right)=1\right]=0.5$ $(0\leq i<m)$. Then the OF of Eq. (23) may be further simplified to

$$\underset{r_0,\cdots,r_{m-1}}{\arg}\min\left\{\sum_{i=0}^{m-1}4^i\cdot T\left(snr,r_i\right)\right\} \quad (25)$$

Moreover, we assume having $snr=5dB$, $R=\frac{1}{3}$, $0.25\leq r_i\leq 1$, while the BER curve LUT $T\left(5dB,r\right)$ of the 3D LUT plane at $snr=5dB$ is displayed in Fig. 5. The objective

[6]The Mathematica tool was employed in the simulations, while more solutions may be found in [43]–[45].

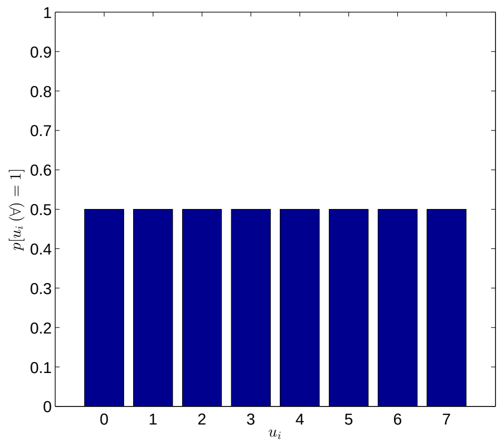

(a) Even distribution of bitplanes

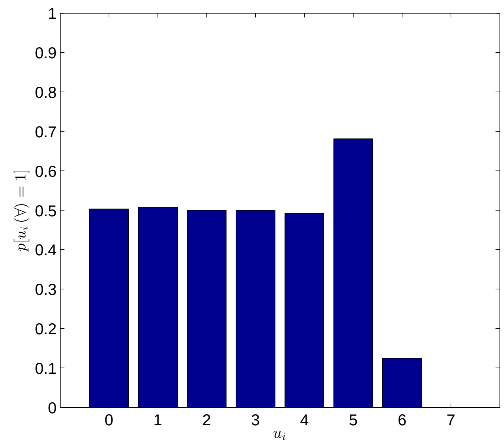

(b) Bitplane distribution of the Coil hologram of [46]

Figure 4: Exemplified graph of $p\left[u_i\left(\forall\right)=1\right]$ $(0\leq i<8)$.

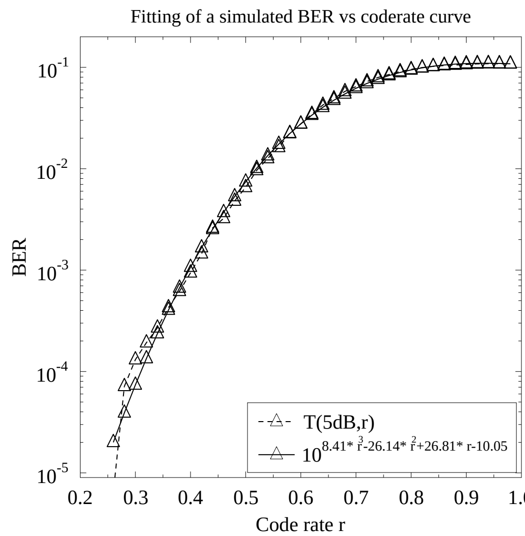

Figure 5: Exemplified BER vs r curve at $snr=5dB$ represented by LUT $T\left(5dB,r\right)$ and the corresponding fitted curve of $10^{8.41\cdot r^3-26.14\cdot r^2+26.81\cdot r-10.05}$.

$$E\left[U(\rho)-\hat{U}(\rho)\right]^2=\sum_{i=0}^{m-1}\sum_{j\in[0,m)}^{j\neq i}2^{i+j}\cdot\{p\left[u_i\left(\rho\right)=1\right]\cdot p\left[u_j\left(\rho\right)=1\right]-2\cdot p\left[u_i\left(\rho\right)=1\right]\cdot p\left[\hat{u}_j\left(\rho\right)=1\right]+p\left[\hat{u}_i\left(\rho\right)=1\right]\}$$
$$+\sum_{i=0}^{m-1}2^{2i}\cdot\{p\left[u_i\left(\rho\right)=1\right]-2\cdot p\left[u_i\left(\rho\right)=1\right]\cdot\left[1-T\left(snr,r_i\right)\right]+p\left[\hat{u}_i\left(\rho\right)=1\right]\} \tag{20}$$

$$E\left[U(\forall)-\hat{U}(\forall)\right]^2=\sum_{i=0}^{m-1}\sum_{j\in[0,m)}^{j\neq i}2^{i+j}\cdot\{p\left[u_i\left(\forall\right)=1\right]\cdot p\left[u_j\left(\forall\right)=1\right]-2\cdot p\left[u_i\left(\forall\right)=1\right]\cdot p\left[\hat{u}_j\left(\forall\right)=1\right]+p\left[\hat{u}_i\left(\forall\right)=1\right]\}$$
$$+\sum_{i=0}^{m-1}2^{2i}\cdot\{p\left[u_i\left(\forall\right)=1\right]-2\cdot p\left[u_i\left(\forall\right)=1\right]\cdot\left[1-T\left(snr,r_i\right)\right]+p\left[\hat{u}_i\left(\forall\right)=1\right]\} \tag{21}$$

function of Eq. (23) may be further simplified to

$$\underset{r_0,\cdots,r_{m-1}}{\arg}\min\left\{\sum_{i=0}^{7}4^i\cdot\exp\left(d+br_i^1+br_i^2+ar_i^3\right)\right\} \tag{26}$$

subject to the constraint of

$$\sum_{i=0}^{7}\frac{1}{r_i}=\frac{8}{1/3} \tag{27}$$

Finally, we obtain the optimal coding rates of $[r_0,\cdots,r_7]=[1,1,1,0.53,0.45,0.39,0.34,0.30]$ by solving Eq. (26), resulting in a minimum MSE of $E\left(MSE\right)=E\left[U(\forall)-\hat{U}(\forall)\right]^2=6.67$ and a minimum of $PSNR_U=39.9dB$, respectively.

D. Complexity Issues

In the Opt-UEP-FEC scheme, the "Coding Rates Optimization" block of Fig. 3 is the only part that imposes overheads compared to the typical equal error protection (EEP) transmission scheme. These overheads include the generation of the LUT $T\left(snr,r\right)$, the estimation of $p\left[u_i\left(\forall\right)=1\right]$ $(0\leq i<m)$ and evaluating the OF of Eq. (23). Among these overheads, the generation of the LUT only imposes extra off-line design-time, while the estimation of $p\left[u_i\left(\forall\right)=1\right]$ $(0\leq i<m)$ and the coding rate optimization impose extra on-line run-time complexity. Additionally, our system may be readily extended to complex-valued holograms, which approximately doubles the run-time complexity. Below, we analyze these complexity issues in order to characterize our system.

1) Generation of LUT $T\left(snr,r\right)$: The LUT $T(snr,r)$ characterizes three components, namely the channel, the transceiver and the FEC codec. Hence this LUT has to be regenerated, when any of these three components is changed. The LUT is independent of the holograms and it is generated during the design process. Furthermore, since the LUT is generated off-line, no extra run-time complexity is imposed by the LUT generation process for different channels, transceivers and FEC schemes. The size of this LUT depends on the number of snr and r values. If n_{snr} and n_r denote the number of snr and r parameters, respectively, the LUT has a size of $(n_{snr}\cdot n_r)$ entries. Furthermore, it costs constant time to generate each entry of the LUT. Hence the complexity depends on the size of the LUT. Overall, the generation of the LUT $T\left(snr,r\right)$ imposes an off-line complexity of $O\left(n_{snr}\cdot n_r\right)$ for time and space.

2) Estimation of $p\left[u_i\left(\forall\right)=1\right]$: For a specific hologram, a one-off scanning is necessitated for estimating $p\left[u_i\left(\forall\right)=1\right]$, which represents a modest complexity. Moreover, the hologram U has size of $(W\times H)$ m-bit pixels. Hence, the estimation of $p\left[u_i\left(\forall\right)=1\right]$ imposes a time complexity of $O\left(W\cdot H\cdot m\right)$ due to one time scanning of the hologram U.

3) Solving the Objective Function: Again, solving the OF of Eq. (23) leads to a multi-dimensional optimization problem, which has been widely studied in the literature [43]–[45]. Specifically, the adaptive particle swarm optimization (APSO) technique of [45] may be readily employed for finding the global optimum in real-time. In our real-time simulations, we employed the Mathematica tool for obtaining the optimal coding rates $r_0,\cdots,r_{m-1}$. In conclusion, the complexity imposed by evaluating the OF depends on the specific multi-dimensional optimization solution employed.

4) Complex-Valued Holograms: For complex-valued holograms, we firstly split each complex pixel into its real and imaginary parts. Then we apply our proposed techniques to the real and imaginary parts, respectively. Hence the complexity of evaluating the objective function is doubled for complex-valued holograms compared to intensity holograms.

V. SIMULATIONS

In this section, we benchmark our proposed Opt-UEP-RSC system against the traditional EEP based FEC (EEP-FEC) system. Specifically, a RSC[7] codec having the hexadecimally represented generator polynomials of $[1011,1101,1101,1111]$ is employed, resulting in the coding rate range of $[0.25,1]$. The overall coding rate of $1/2$ was employed. Moreover, BPSK

[7]A recursive systematic convolutional (RSC) [47] code retains the original information bits in the encoded sequence and additionally incorporates the parity bits. These parity bits are generated with the aid of a so-called recursive generator polynomial, which indicates that this encoder feeds back the parity bits for the computation of future parity bits. The benefits of this feedback is that the encoder has an infinite memory, which hence efficiently spreads the parity information over the encoded stream and therefore improves the decoding performance attained.

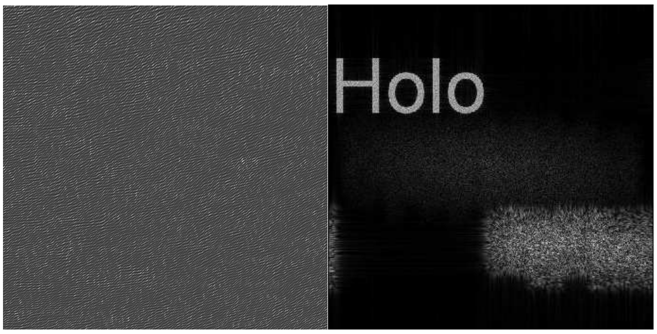

(a) Hologram of *Holo* (b) Reconstructed image of the *Holo* Hologram

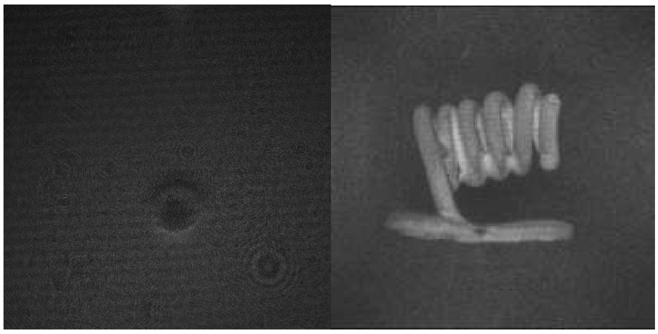

(c) Hologram of *Coil* (d) Reconstructed image of the *Coil* Hologram

Figure 6: The Holo and Coil holograms employed.

	Holo	Coil
Representation	YUV 4:0:0	YUV 4:0:0
Format	256×256	2048×2032
Bit-depth	8	8
Type	CGH	DH
Wavelength	532nm	633nm
Coding rates	0.25~1	0.25~1
Overall coding rate	1/2	1/2

Table III: The parameters of the holograms employed.

snr	r	ber
⋮	⋮	⋮
0	0.26	0.014
0	0.28	0.035
0	0.30	0.046
⋮	⋮	⋮
0.5	0.26	0.008
0.5	0.28	0.022
0.5	0.30	0.030
⋮	⋮	⋮

Table IV: Example of the LUT $T\,(snr, r)$.

modulated signals were transmitted through *non-dispersive uncorrelated Rayleigh fading wireless channels*.

We employ the $m = 8$ bit-depth intensity Holo and Coil holograms. seen in Fig. 6, which are formatted in 4:0:0 YUV and represented in (256×256)- and (2048×2032)-pixel formats, respectively. The Holo hologram was generated by CGH using a laser wavelength of 532 nm at a distance of 1.5 m, while the Coil hologram [46] was digitally recorded using a laser wavelength of 633 nm. The parameters of the holograms employed are listed in Table III. In all of our experiments, each hologram was transmitted 100 times in order to generate statistically sound performance curves.

A. Off-line LUT Generation

In our experiments, the vectors of $[0 : 0.5 : 15]$ and $[0.26 : 0.02 : 1]$[8] are utilized for the variables snr and r, respectively, for generating the LUT, which result in $n_{snr} = 31$, $n_r = 38$. For each snr value of $T\,(snr, r)$, we recorded the BER achieved by the RSC decoder for the coding rates of $[0.26 : 0.02 : 1]$. Furthermore, 8-byte floating values were utilized for storing the LUT in memory. Correspondingly, the LUT $T\,(snr, r)$ requires memory sizes of about $(n_{snr} \times n_r) =$ 1178 bytes. Some of the LUT entries generated for our system are displayed in Table IV.

B. System Performance

In this section, we benchmark our Opt-UEP-RSC system against the traditional EEP-RSC system. The BER versus E_b/N_0 curves of the eight bitplanes of the Holo hologram are displayed in Fig. 7a. As expected, the BER of the bitplanes $u_4, \cdots, u_7$ of the Opt-UEP-RSC system is always better than that of the EEP-RSC system, while the BER of the bitplanes $u_0, \cdots, u_3$ is worse than that of the EEP-RSC system owing to the specific code rates. More specifically, this is due to the fact that the coding-rates of the bitplanes $u_0, \cdots, u_3$ are increased for the sake of protecting the more vunerable $u_4, \cdots, u_7$ bitplanes. Similar trends were observed also for the Coil hologram, which are displayed in Fig. 7d.

The PSNR versus E_b/N_0 performance recorded for the Holo hologram is displayed in Fig. 7b, where the PSNR estimated using the techniques detailed in Section IV is also provided by the curve Opt-UEP-RSC-Est. We observe that the Opt-UEP-RSC scheme substantially outperforms the EEP-RSC system, while it has similar performance to the theoretical curve Opt-UEP-RSC-Est. Specifically, the Opt-UEP-RSC scheme achieves an E_b/N_0 reduction of about 2.6 dB compared to the EEP-RSC scheme at a PSNR of 48 dB[9]. Alternatively, about 12.5 dB of PSNR hologram quality improvement is observed at an E_b/N_0 of 7 dB. Furthermore, the PSNR versus E_b/N_0 performance of the Opt-UEP-RSC

[8]These values can be stored as floats in 8 bytes each. the first and last element represent the interval limits, while the one in the middle is the step-size.

[9]48 dB represents that the signal is near losslessly received.

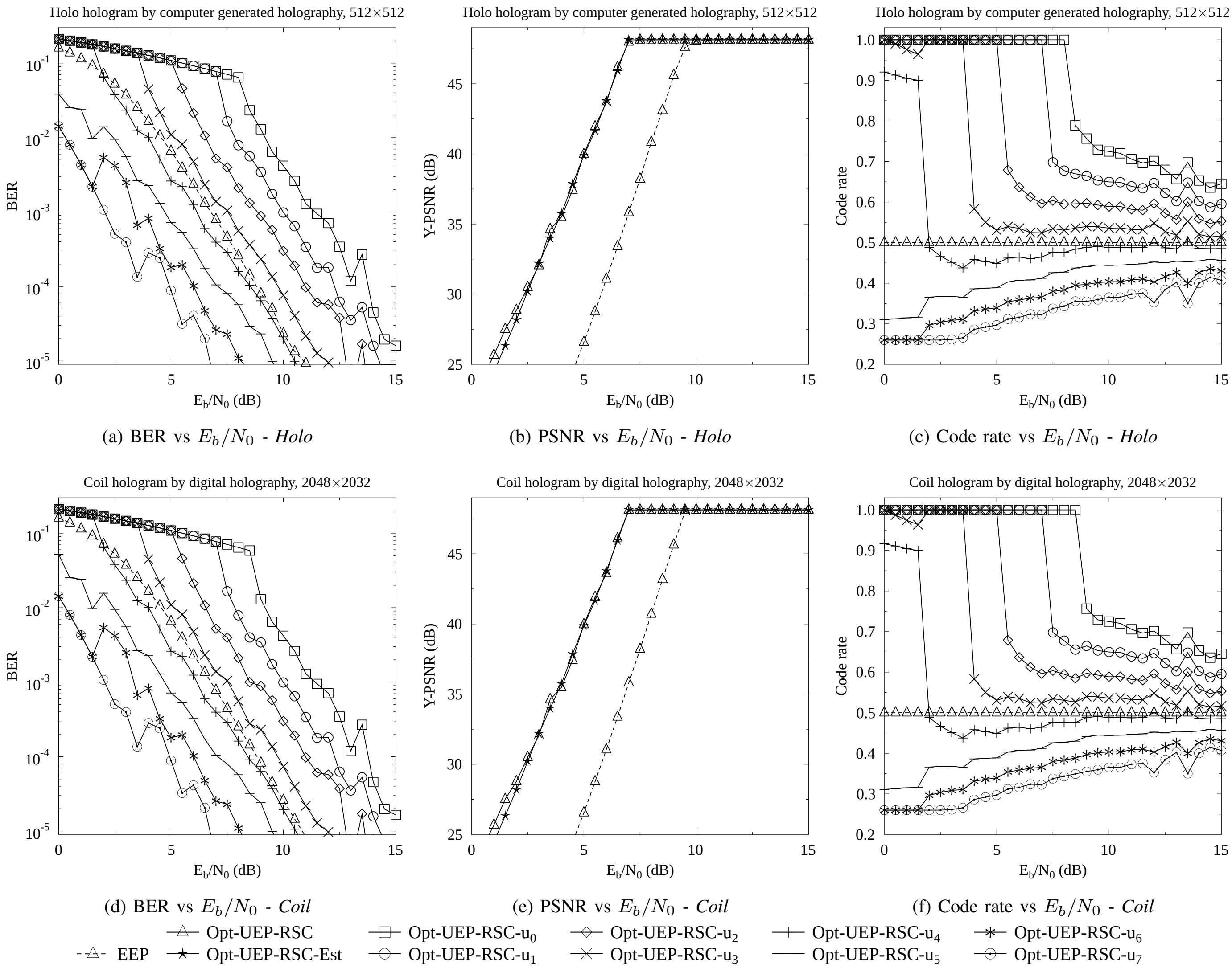

(a) BER vs E_b/N_0 - *Holo* (b) PSNR vs E_b/N_0 - *Holo* (c) Code rate vs E_b/N_0 - *Holo*

(d) BER vs E_b/N_0 - *Coil* (e) PSNR vs E_b/N_0 - *Coil* (f) Code rate vs E_b/N_0 - *Coil*

Figure 7: BER, PSNR, Code rate versus E_b/N_0 performance comparison of the proposed system and the benchmarkers, namely the EEP-RSC scheme, the Opt-UEP-RSC scheme and the Opt-UEP-RSC-Est scheme for the *Holo* and *Coil* holograms.

using the Coil hologram is portrayed in Fig. 7e, where similar trends to those of Fig. 7b were observed. A subjective comparison of the benchmarkers recorded for the Holo hologram is presented in Fig. 8. In the first row, the three columns (from left to right) indicate the original hologram as well as that of the EEP-RSC scheme and of the Opt-UEP-RSC scheme, respectively. In the second row, the first/second figure indicates the difference between the original and the EEP-RSC/Opt-UEP-RSC decoded hologram.

C. Optimized Coding Rates

The optimized coding rates found by our proposed regime for the Holo and Coil holograms are shown in Figs. 7c and 7f, respectively. Specifically, the y axis of Figs. 7c and 7f indicates the coding rates. Observe from Fig. 7c that the coding rates $r_4, \cdots, r_7$ found for the bitplanes $u_4, \cdots, u_7$ increase gradually as the E_b/N_0 increases, while opposite trends were observed for the coding rates $r_0, \cdots, r_3$. This is due to the fact the bitplanes $u_0, \cdots, u_3$ were protected less well for the sake of protecting the more important bitplanes $u_4, \cdots, u_7$ at lower E_b/N_0 values. At high E_b/N_0 values, more RSC protection bits were allocated to the less important bitplanes $u_0, \cdots, u_3$, since better channel conditions result in a lower BER of the bitplanes $u_4, \cdots, u_7$, which freed up part of the RSC protection bits reassigned from the bitplanes $u_0, \cdots, u_3$. Similar trends may be observed for the Coil hologram, as displayed in Fig. 7f.

VI. Conclusions

We proposed a UEP-FEC technique for the bitplane based transmission of digital holograms over wireless channels, where the coding rates of different bitplanes were optimized for the sake of achieving an improved hologram quality. Firstly, the transceiver and soft-decoded FEC are treated as a black box, which was modeled by a LUT. Then the PSNR of the hologram decoded at the receiver was expressed as

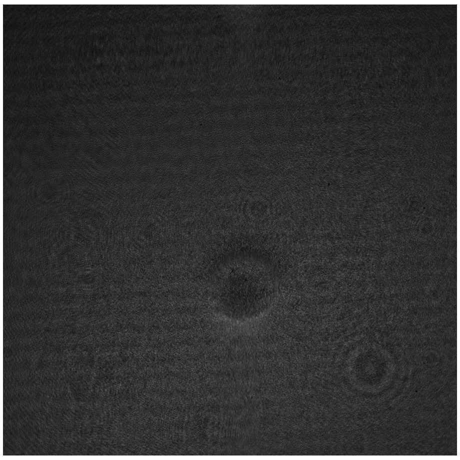

(a) Original

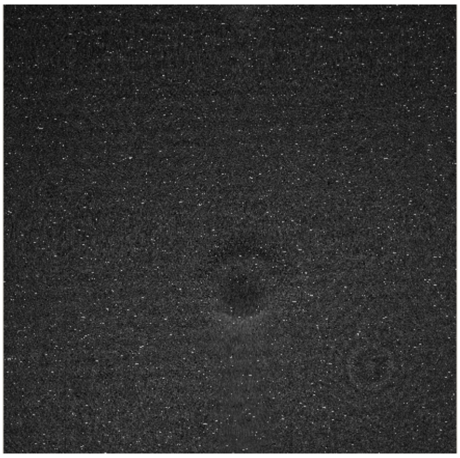

(b) EEP-RSC

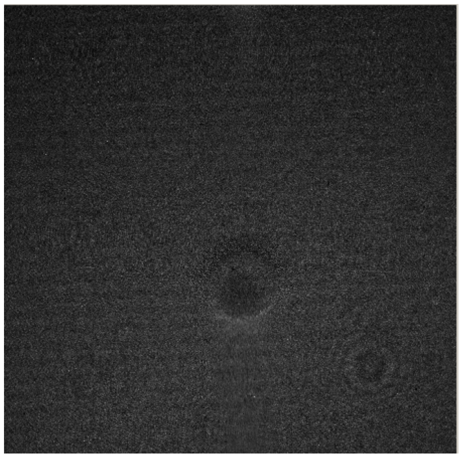

(c) Opt-UEP-RSC

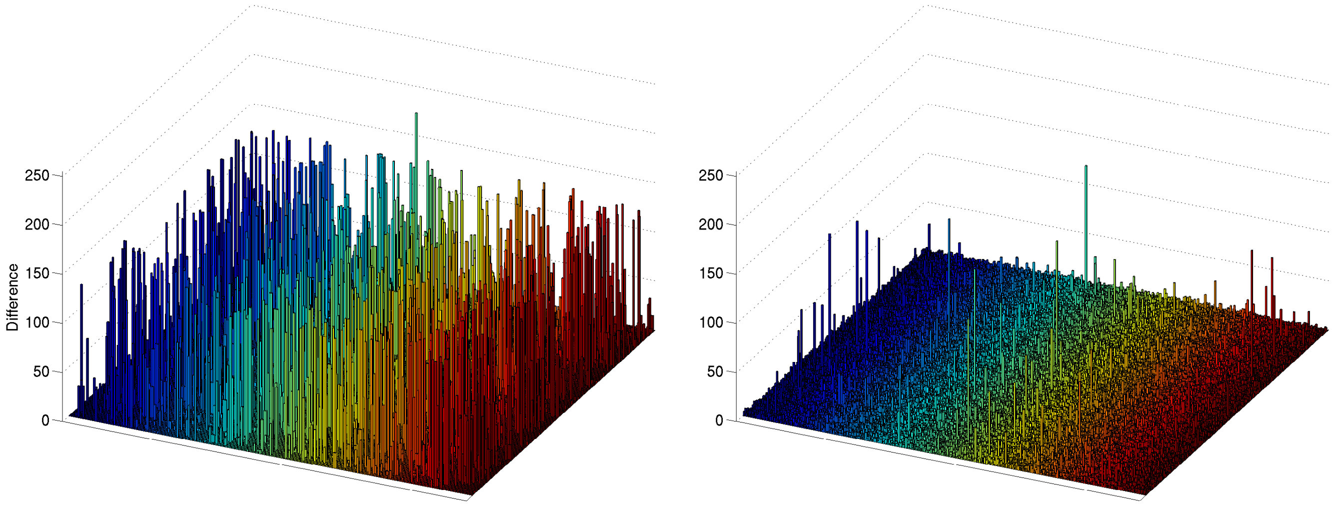

(d) Comparison of difference between original and decoded holograms

Figure 8: Comparison of the frames at E_b/N_0 of 5 dB for the *Coil* hologram.

a function of FEC coding rates of the m independently encoded bitplanes. Finally, we solved the resultant multi-dimensional optimization problem of generating the optimal coding rates for the m bitplanes. Numerical simulation of a pair of holograms were provided, which shows that the proposed Opt-UEP-FEC system outperforms the traditional UEP-FEC system by up to 2.6 dB of E_b/N_0 or 12.5 dB of PSNR, when employing a RSC code.

In our future work, we may incorporate our previous inter-layer FEC technique [37], [38] into our digital hologram transmission system. Moreover, we may consider compressing the digital holograms using lossless variable length coding (VLC) [48], [49], which is capable of soft decoding.

References

[1] D. Gabor, "A new microscopic principle," *Nature*, vol. 161, pp. 777–778, May 1948.

[2] N. Pandey and B. Hennelly, "Quantization noise and its reduction in lensless Fourier digital holography," *Appled Optics*, vol. 50, pp. B58–B70, March 2011.

[3] M. Lin, K. Nitta, O. Matoba, and Y. Awatsuji, "Parallel phase-shifting digital holography with adaptive function using phase-mode spatial light modulator," *Appled Optics*, vol. 51, pp. 2633–2637, May 2012.

[4] Y. Ohsawa, K. Yamaguchi, T. Ichikawa, and Y. Sakamoto, "Computer-generated holograms using multiview images captured by a small number of sparsely arranged cameras," *Appled Optics*, vol. 52, pp. A167–A176, January 2013.

[5] L. Huang, X. Chen, H. Mühlenbernd, H. Zhang, S. Chen, B. Bai, Q. Tan, G. Jin, K.-W. Cheah, C.-W. Qiu, J. Li, T. Zentgraf, and S. Zhang, "Three-dimensional optical holography using a plasmonic metasurface," *Nature Communications*, vol. 4, November 2013.

[6] B. J. Jackin and T. Yatagai, "Fast calculation of spherical computer generated hologram using spherical wave spectrum method," *Optics Express*, vol. 21, pp. 935–948, January 2013.

[7] L. Onural, F. YarasÌ§, and H. Kang, "Digital holographic three-dimensional video displays," *Proceedings of the IEEE*, vol. 99, pp. 576–589, April 2011.

[8] Y. N. Denisyuk, "Photographic reconstruction of the optical properties of an object in its own scattered radiation field," *Soviet Physics Doklady*, vol. 7, pp. 543–545, 1962.

[9] E. N. Leith and J. Upatnieks, "Wavefront reconstruction with diffused illumination and three-dimensional objects," *Journal of the Optical Society of America B*, vol. 54, pp. 1295–1301, November 1964.

[10] B. R. Brown and A. W. Lohmann, "Complex spatial filtering with binary masks," *Applied Optics*, vol. 5, pp. 967–969, June 1966.

[11] A. W. Lohmann and D. P. Paris, "Binary Fraunhofer holograms, generated by computer," *Applied Optics*, vol. 6, pp. 1739–48, October 1967.

[12] J. W. Goodman and R. W. Lawrence, "Digital image formation from electronically detected holograms," *Applied Physics Letters*, vol. 11, pp. 77–79, 1967.

[13] M. K. Kim, "Principles and techniques of digital holographic microscopy," *Journal of Photonics for Energy*, pp. 018005–018005–50, 2010.

[14] L. Yaroslavskii and N. Merzlyakov, *Methods of Digital Holography*. Consultants Bureau, 1980.

[15] U. Schnars and W. Jüptner, *Digital Holography: Digital Hologram Recording, Numerical Reconstruction, and Related Techniques*. Springer, 2005.

[16] I. Moon, M. Daneshpanah, B. Javidi, and A. Stern, "Automated three-dimensional identification and tracking of micro/nanobiological organisms by computational holographic microscopy," *Proceedings of the IEEE*, vol. 97, pp. 990–1010, June 2009.

[17] G. Pedrini, M. Gusev, S. Schedin, and H. Tiziani, "Pulsed digital holographic interferometry by using a flexible fiber endoscope," *Optics and Lasers in Engineering*, vol. 40, pp. 487–499, November 2003.

[18] R. Gazdzinski and L. Rosen, "Error-corrected wideband holographic communications apparatus and methods," May 2005. US Patent Application 10/867,794.

[19] Y. Huo, C. Hellge, T. Wiegand, and L. Hanzo, "A tutorial and review on inter-layer FEC coded layered video streaming," *IEEE Communications Surveys Tutorials*, vol. 17, pp. 1166–1207, 2nd-quarter 2015.

[20] Y. Frauel, T. Naughton, O. Matoba, E. Tajahuerce, and B. Javidi, "Three-dimensional imaging and processing using computational holographic imaging," *Proceedings of the IEEE*, vol. 94, pp. 636–653, March 2006.

[21] L. Onural, A. Gotchev, H. Ozaktas, and E. Stoykova, "A survey of signal processing problems and tools in holographic three-dimensional television," *IEEE Transactions on Circuits and Systems for Video Technology,*, vol. 17, pp. 1631–1646, November 2007.

[22] T. J. Naughton, J. B. McDonald, and B. Javidi, "Efficient compression of fresnel fields for internet transmission of three-dimensional images," *Appled Optics*, vol. 42, pp. 4758–4764, August 2003.

[23] M. Liebling, T. Blu, and M. Unser, "Fresnelets: new multiresolution wavelet bases for digital holography," *IEEE Transactions on Image Processing*, vol. 12, pp. 29–43, January 2003.

[24] E. Darakis and J. Soraghan, "Use of fresnelets for phase-shifting digital hologram compression," *IEEE Transactions on Image Processing*, vol. 15, pp. 3804–3811, December 2006.

[25] A. Shortt, T. J. Naughton, and B. Javidi, "Compression of digital holograms of three-dimensional objects using wavelets," *Optics Express*, vol. 14, pp. 2625–2630, April 2006.

[26] L. T. Bang, Z. Ali, P. D. Quang, J.-H. Park, and N. Kim, "Compression of digital hologram for three-dimensional object using wavelet-bandelets transform," *Optics Express*, vol. 19, pp. 8019–8031, April 2011.

[27] H. Schwarz, D. Marpe, and T. Wiegand, "Overview of the scalable video coding extension of the H.264/AVC standard," *IEEE Transactions on Circuits and Systems for Video Technology*, vol. 17, pp. 1103–1120, September 2007.

[28] Y.-H. Seo, Y.-H. Lee, J.-S. Yoo, and D.-W. Kim, "Scalable hologram video coding for adaptive transmitting service," *Appled Optics*, vol. 52, pp. A254–A268, January 2013.

[29] K. Takano, K. Sato, T. Endo, H. Asano, A. Fukuzawa, and K. Asai, "An elementary research on wireless transmission of holographic 3D moving pictures," *Proc. SPIE*, vol. 7358, pp. 73581A–73581A–11, May 2009.

[30] R. D. Leonardo and S. Bianchi, "Hologram transmission through multi-mode optical fibers," *Optics Express*, vol. 19, pp. 247–254, January 2011.

[31] K. Sato, M. Tozuka, K. Takano, and M. Ohki, "Transmission of hologram data and 3D image reconstruction using white LED light," *Proc. SPIE*, vol. 8281, pp. 82810A–82810A–6, 2012.

[32] M. Tozuka, K. Takano, K. Sato, and M. Ohki, "Digital space transmission of an interference fringe-type computer-generated hologram using IrSimple," *Proceedings of ITU Kaleidoscope: Building Sustainable Communities (K-2013)*, pp. 1–6, April 2013.

[33] Y. Huo, C. Zhu, and L. Hanzo, "Spatio-temporal iterative source-channel decoding aided video transmission," *IEEE Transactions on Vehicular Technology*, vol. 62, pp. 1597–1609, May 2013.

[34] Y. Huo, T. Wang, R. G. Maunder, and L. Hanzo, "Iterative source and channel decoding relying on correlation modelling for wireless video transmission," *IET Communications*, vol. 7, pp. 1465–1475, September 2013.

[35] ITU, *Joint Photographic Experts Group ISO/IEC, JTC/SC/WG8, CCITT SGVIII. JPEG technical specifications, revision 5. Report JPEG-8-R5*, January 1990.

[36] Joint Video Team (JVT) of ISO/IEC MPEG and ITU-T VCEG, *ITU-T Rec. H.264/ISO/IEC 14496-10 AVC: Advanced Video Coding for Generic Audiovisual Services*, March 2010.

[37] Y. Huo, M. El-Hajjar, R. G. Maunder, and L. Hanzo, "Layered wireless video relying on minimum-distortion inter-layer FEC coding," *IEEE Transactions on Multimedia*, vol. 23, pp. 319–331, January 2014.

[38] Y. Huo, M. El-Hajjar, and L. Hanzo, "Inter-layer FEC aided unequal error protection for multilayer video transmission in mobile TV," *IEEE Transactions on Circuits and Systems for Video Technology*, vol. 23, pp. 1622–1634, September 2013.

[39] Y. Huo, C. Hellge, T. Wiegand, and L. Hanzo, "A tutorial and review on inter-layer FEC coded layered video streaming," *IEEE Communications Surveys and Tutorials*, vol. 17, pp. 1166–1207, 2nd-quarter 2015.

[40] T. Poon, *Digital Holography and Three-Dimensional Display: Principles and Applications*. Springer, 2006.

[41] P. Picart and J. Li, *Digital Holography*. ISTE, Wiley, 2013.

[42] Q. Huynh-Thu and M. Ghanbari, "Scope of validity of PSNR in image/video quality assessment," *Electronics Letters*, vol. 44, pp. 800–801, June 2008.

[43] M. Clerc and J. Kennedy, "The particle swarm - explosion, stability, and convergence in a multidimensional complex space," *IEEE Transactions on Evolutionary Computation*, vol. 6, no. 1, pp. 58–73, 2002.

[44] D. Schonfeld and N. Bouaynaya, "A new method for multidimensional optimization and its application in image and video processing," *IEEE Signal Processing Letters*, vol. 13, no. 8, pp. 485–488, 2006.

[45] Z.-H. Zhan, J. Zhang, Y. Li, and H.-H. Chung, "Adaptive particle swarm optimization," *IEEE Transactions on Systems, Man, and Cybernetics, Part B: Cybernetics*, vol. 39, pp. 1362–1381, December 2009.

[46] E. Darakis, M. Kowiel, R. Näsänen, and T. J. Naughton, "Visually lossless compression of digital hologram sequences," *Proceedings of SPIE*, vol. 7529, pp. 752912–752912–8, 2010.

[47] C. Berrou and A. Glavieux, "Near optimum error correcting coding and decoding: Turbo codes," *IEEE Transactions on Communications*, vol. 44, pp. 1261–1271, October 1996.

[48] L. Hanzo, P. Cherriman, and J. Streit, *Video Compression and Communications: From Basics to H.261, H.263, H.264, MPEG2, MPEG4 for DVB and HSDPA-Style Adaptive Turbo-Transceivers*. New York: John Wiley, 2007.

[49] L. Hanzo, R. G. Maunder, J. Wang, and L.-L. Yang, *Near-Capacity Variable-Length Coding: Regular and Exit-Chart Aided Irregular Designs*. John Wiley & Sons Ltd, 2010.

Yongkai Huo received the B.Eng. degree with distinction in computer science and technology from Hefei University of Technology, Hefei, China, in 2006 and the M.Eng. degree in computer software and theory from University of Science and Technology of China, Hefei, China, in 2009. In 2014, he was awarded a Ph.D in Wireless Communications group, School of Electronics and Computer Science, University of Southampton, Southampton, UK, where he continued to work as a research fellow until September 2016. He received a scholarship under the China-U.K. Scholarships for Excellence Programme. He is now an associate professor with the College of Computer Science&Software Engineering, Shenzhen University, China. He has published a number of research papers in holographic images, distributed video coding, multiview video coding, robust wireless video streaming and joint source-channel decoding etc.

Péter Tamás Kovács (Student member, IEEE) received the M.Sc. degree in computer science from the Budapest University of Technology, Budapest, Hungary in 2004. He is currently pursuing the Ph.D. degree in signal processing at Tampere University of technology, Tampere, Finland. From 2004 to 2006, he was a Software Engineer with Archi-Data. Since 2006, he has been Software Engineer, Lead Software Engineer, then CTO of Holografika. He has been a visiting researcher at Tampere University of Technology from 2013 to 2014. He is the author or co-author of three book chapters, three journal papers and more than 30 conference papers. His research interests include 3D displays, more specifically light-field displays, and the capture / compression / rendering of light fields. He has served as Program Committee member for numerous international IEEE conferences, Local Organizing Chair of 3DTV-Con 2014, and is a contributing member of the International 3D Society and the International Committee for Display Metrology (ICDM), where he contributed to the first IDMS standard. He was the Head of Delegation to MPEG for Hungary. He also served as the chair of the Working Group 5 ("3D End-User Devices") of 3D-ConTourNet COST Action.

Thomas J. Naughton is a Professor in the Maynooth University Department of Computer Science. His research and teaching areas are related to digital holography, optical image processing, and computer theory. During 2008-2011 he was Coordinator and Scientific Leader of the 40-person-year European Commission FP7 Collaborative Project about digital holography called "Real 3D." During 2007-2009 he was a European Commission Marie Curie Fellow based in University of Oulu, Finland. He was jointly awarded the IEEE Donald G. Fink Prize Paper Award in 2008.

Lajos Hanzo (F' 04), Fellow of EURASIP, DSc received his degree in electronics in 1976 and his doctorate in 1983. In 2009 he was awarded an honorary doctorate by the Technical University of Budapest and in 2015 by the University of Edinburgh. In 2016 he was admitted to the Hungarian Academy of Science. During his 40-year career in telecommunications he has held various research and academic posts in Hungary, Germany and the UK. Since 1986 he has been with the School of Electronics and Computer Science, University of Southampton, UK, where he holds the chair in telecommunications. He has successfully supervised 100+ PhD students, co-authored 18 John Wiley/IEEE Press books on mobile radio communications totalling in excess of 10 000 pages, published 1600+ research contributions at IEEE Xplore, acted both as TPC and General Chair of IEEE conferences, presented keynote lectures and has been awarded a number of distinctions. Currently he is directing a 60-strong academic research team, working on a range of research projects in the field of wireless multimedia communications sponsored by industry, the Engineering and Physical Sciences Research Council (EPSRC) UK, the European Research Council's Advanced Fellow Grant and the Royal Society's Wolfson Research Merit Award. He is an enthusiastic supporter of industrial and academic liaison and he offers a range of industrial courses. He is also a Governor of the IEEE VTS. During 2008 - 2012 he was the Editor-in-Chief of the IEEE Press and a Chaired Professor also at Tsinghua University, Beijing. For further information on research in progress and associated publications please refer to http://www-mobile.ecs.soton.ac.uk Lajos has 27 000+ citations and an H-index of 63.